sciendo

Int. J. of Applied Mechanics and Engineering, 2022, vol.27, No.4, pp.13-25
DOI: 10.2478/ijame-2022-0047

OPTIMIZATION OF FRICTION STIR PROCESSING PARAMETERS OF ALUMINUM ALLOY REINFORCED WITH HYBRID NANOPARTICLES USING THE TAGUCHI METHOD

Mohammed Sultan ALI* and Iman Q. Al SAFFAR
University of Baghdad, College of Engineering, Department of Mechanical Engineering, IRAQ
E-mail: Mohammed.Ali2003M@coeng.uobaghdad.edu.iq

This study deals with the selection of optimum parameters for friction stir processing of Al alloy 6061-T6 reinforced with a hybrid nanoparticle (B4C and SiO2) in terms of their effect on the mechanical properties (hardness, tensile strength, and wear resistance) using Taguchi method. This work was carried out under four parameters each one running in three levels; rotational speeds (*800*, *1000* and *1200*) rpm, travel speeds (*10*, *20*, and *30*) mm/min, holes depth (*2*, *2.5*, and *3*) *mm*, and mixing ratio of (SiO2/B4C) nanoparticles (*1/1*, *1/2*, and *1/3*), using *L9* (*34*) Taguchi orthogonal array. Tensile strength and microhardness tests were conducted to evaluate the mechanical properties, in addition to the wear resistance test which is carried out using a pin-on-disk device. The microstructure was examined by optical microscopy, field emission scanning electron microscopy, and x-ray diffraction analysis. It was found that the highest tensile strength (*223*) *MPa* at *1200 rpm* rotational speed, *30 mm/min* traverse speed, *2.5 mm* holes depth, and *1/2* (SiO2/B4C) nanoparticles mixing ratio, the highest hardness reached is (*155*) HV, then decreases in the direction of thermomechanically affected zone (TMAZ), heat affected zone (HAZ), and the base material at (*1200*) *rpm* rotational speed, (*30*) mm/min linear speed, a hole depth of (*2*) mm and (*1/3*) mixing ratio of (B4C/SiO2) nanoparticles. The wear behavior was of a mild type or an oxidative type at low loads (*5 N*), which became severe or metallic wear at higher loads (*20 N*) at fixed sliding time and speed. The (ANOVA) table has been used to determine which parameter is the most significant using MINITAB software.

Keywords: aluminum alloy, friction stir processing, nanoparticles, Taguchi method, ANOVA.

1. Introduction

Aluminum alloys are useful in a variety of industries, including aerospace and automotive, due to their unique properties of lightweight and high strength-to-weight ratio [1]. Aluminum alloy 6061-T6 is frequently utilized in maritime, automotive and aircraft industries due to its good features of low density, good strength, and strong erosion and corrosion properties [2]. Improved mechanical properties are obtained by homogenizing and grain structure refining of the alloy. Thermomechanical treatment (TMT), high-pressure torsion (HPT), equal channel angular procedure (ECAP), accumulative roll bonding (ARB), and other methods are used to achieve this. These methods are time-consuming and complicated [3]. Friction Stir Processing (FSP), a new grain refining technique, and fabrication of surface has been recently developed. Its fundamental ideas are identical to those of FSW. FSP appears to be a promising strategy for improving metal characteristics [4, 5]. A rotary tool with a threaded pin attaches to the surface of the metal to be processed via FSP and traverses through the routes. The friction between the metal surface, the revolving shoulder, and the threaded pin will generate heat. The metal's temperature does not exceed the melting point; just a plastic deformation emerges in the processing zone [6]. There are numerous advantages of FSP. FSP is a single-step solid-state method that achieves homogeneity and microstructural refinement in a fast route. Furthermore, friction and plastic deformation lead to heat generation during friction stir processing, implying that FSP is environmentally favorable and a low-energy technique with no radiation, noise, or harmful gases FSP [7].

* To whom correspondence should be addressed

Taguchi technique was applied to architectural analysis on a wide scale, and it is extensively employed in building high-quality systems to explore the influence of FSP parameters by performing minimal experiments [8]. Kwon *et al.* [9] discovered that applying FSP to 1050 Al alloy improved the mechanical properties such as the tensile strength and hardness as the rotational speed was reduced. In comparison to the base alloy, these characteristics rose by almost 37 percent and 46 percent at *560 rpm* due to grain improvements.

Balasubramanian and Elangovan [10] investigated the effects of FSP factors (rotation speed and pin profile) on aluminum alloy 2219 with *6 mm* thickness. To make the weld, three different tool rotating speeds were used with five different pin profiles (triangular, threaded cylindrical, square, straight cylindrical, and tapered cylindrical). In comparison to other tool pin profiles, they determined that the best pin profile was the square tool due to its ability to generate sound and metallurgically defect-free welds.

FSP was utilized by Shafiei Zarghani *et al.* [11] to manufacture ultra-fine-grained metals using rigorous plastic deformations. FSP was used to extrude 6082-T4 aluminum alloy to produce very tiny-grained microstructures with grain sizes ranging from *0.5* μ*m* to *3* μ*m*. The hardness of the FSPed aluminum alloy grows significantly as the tool rotation speed is reduced.

Magdy *et al.* [12] used FSP to improve the mechanical characteristics and change the microstructure of 6082-T6 aluminum alloy. Processing was done at a set rotation speed (*850rpm*) and three different traverse speeds (*90, 140, 224*) *mm/min* higher traverse speed resulted in increased strength and microhardness, while increasing the pass number led to decreased softening and tensile strength.

Muna K. Abbassa and Noor Alhuda B. Sharhana [13] studied the optimization of FSP parameters that affect the tensile strength of AA6061 *6 mm* plate reinforced with microparticles of Al2O3 and SiC using the Taguchi method. They suggest three parameters each one running in three levels, rotational speed (*800, 100, 1200*) *rpm*, transverse speed (*16, 25, 30*) *mm/min*, and the number of passes (*1, 2, 3*), tool tilt angle *2.5*° using a cylindrical threaded pin. They found that the optimum FSP parameters were *1250 rpm* rotational speed, *32 mm/min* transverse speed, and two passes in the same direction, and that the higher hardness value was *75HV* in stir zone center and then decreased toward the TMAZ, HAZ, and the base metal.

The goal of this research is to find the ideal FSP parameters, which include tool rotation speed, travel speed, depth of holes, and the mixing ratio of (B4C/SiO2) nanoparticles. The L9 Taguchi orthogonal array is used to identify the most effective friction stir processing parameters. ANOVA was also used to determine the contribution of each parameter to the overall process.

2. Experimental work

A CNC cutting machine was used to cut a plate mode of 6061-T6 Al alloy (which is used in this research) into $(5\times100\times150)$ *mm* in dimensions. Spectro-meter analytical equipment was used to determine the chemical structure of the base metal as shown in Tab.1, whereas Tab.2 shows the standard and measured mechanical properties of the as-received 6061-T6 alloy.

Table 1. Base metal 6061-T6 Al alloy chemical composition.

Elements	Si	Cu	Mg	Cr	Ni	Ti	Fi	Zn	Mn	Other	Al
Standard	*0.71 max.*	*0.4 max.*	*1.2 max.*	*0.35 max.*	*0.05 max.*	*0.15 max.*	*0.80 max.*	*0.25 max.*	*0.15 max.*	*0.80 max.*	*bal.*
Base metal	*0.38*	*0.07*	*1.2*	*0.21*	*0.001*	*0.03*	*0.30*	*0.11*	*0.80*	*0.20*	*bal.*

Table 2. 6061-T6 Al alloy mechanical properties.

6061-T6 Al Alloy	YS (*MPa*)	TS (*MPa*)	E (%)	Hardness *HV*
Measured	*248*	*294*	*8.35*	*65*
Standard	*275*	*311*	*12*	*94*

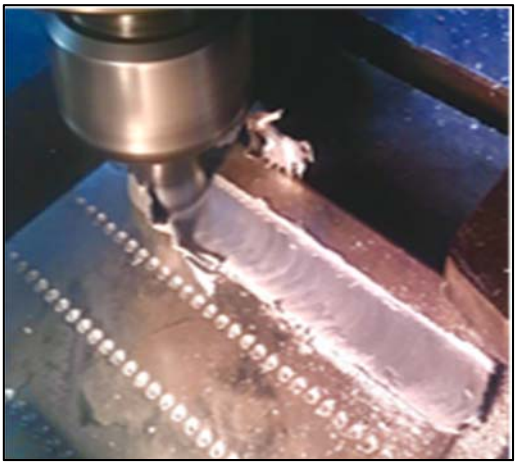

Fig.1. Samples during FSP.

Fig.2. Cylindrical shoulder with threaded pin.

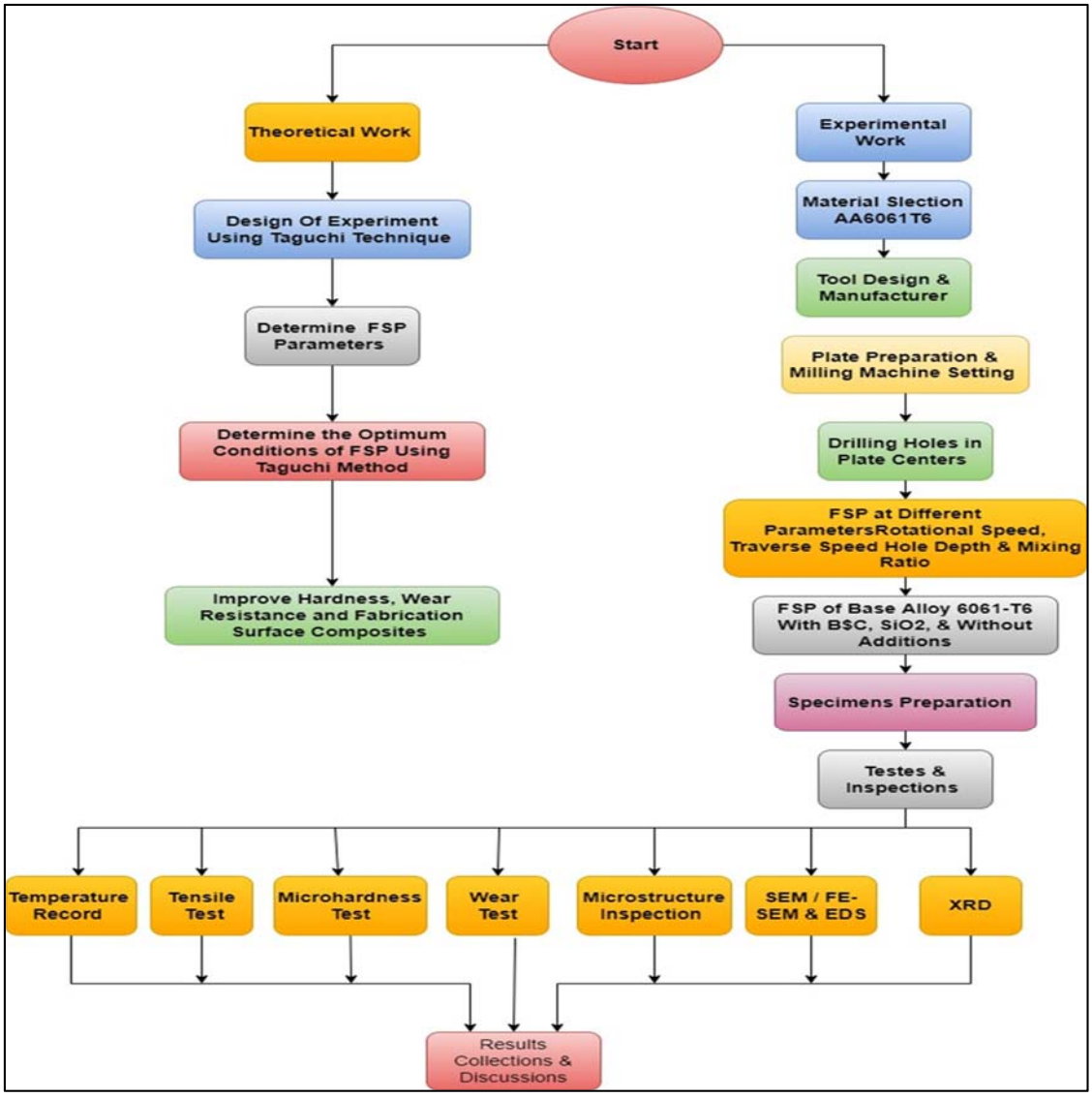

Fig.3. Flow chart explains the steeps sequence of the study.

A vertical-type CNC milling machine (MARUFUKU JAPAN) was used to perform the friction stir processing. Specimens were prepared and secured tightly in fixtures designed especially for this purpose to make sure that the work pieces stay in place and do not move due to friction stresses, then the tool has been plunged into the plate at a fixed plunging depth, and the tool tilt angle of *0.3 mm* and *2.5*°, respectively, as illustrated in Fig.1.

Noor Zaman Khan, *et al.* [14] found that the best ratio of shoulder to pin diameter *D/d* for AA6061 is *3*. Based on this result, a non-consumable tool of a cylindrical shoulder with a threaded of *24 mm* in diameter of shoulder and (*8*, *3*) *mm* pin's diameter and length, respectively, was manufactured from a high-speed steel shaft, as shown in Fig.2.

A series of holes were created in the work-piece center line for the addition of nanoparticles, and the spacing between each two holes was *1.5 mm*, each hole was of *2 mm* in diameter and *3* different depth of (*2, 2.5, and 3*) mm. There were *40* holes at length *140 mm*, made via the CNC vertical milling machine mentioned above. Figure 3 shows the flow chart of this work.

3. Orthogonal array selection

Taguchi's experimental design includes the use of an orthogonal array to set the factors and levels of friction stir processing. Each set of process parameters was subjected to three experiments by Taguchi's *L9* orthogonal array proposal. The rotational speed (*rpm*), transverse speeds (*mm/min*), depth of holes, and the mixing ratio of (B4C/SiO2) nanoparticles were the four characteristics considered in this study. The characteristics and levels of the procedure are shown in Tab.3. The tilt angle (*2.5*°) does not change. Table 3 shows the results of a total of "nine experimental" runs, each with a different set of levels for each parameter.

Table 3. FSP levels and parameters.

Factors	Level 1	Level 2	Level 3
Rotational speed (*rpm*)	*800*	*1000*	*1200*
Travers speed (*mm/min*)	*10*	*20*	*30*
Depth of holes (*mm*)	*3*	*2.5*	*2*
Mixing ratio	*1/1*	*1/2*	*1/3*

Table 4. L_9 (3^4) Taguchi orthogonal array design.

Experiment No.	Rotational speed (rpm)	Travers speed (mm/min)	Holes depth (mm)	Mixing ratio
1	*800*	*10*	*2*	*1/1*
2	*800*	*20*	*2.5*	*1/2*
3	*800*	*30*	*3*	*1/3*
4	*1000*	*10*	*2.5*	*1/3*
5	*1000*	*20*	*3*	*1/1*
6	*1000*	*30*	*2*	*1/2*
7	*1200*	*10*	*3*	*1/2*
8	*1200*	*20*	*2*	*1/3*
9	*1200*	*30*	*2.5*	*1/1*

Tensile, microhardness, and wear tests were made after friction stir processing to estimate the properties of FSP for each parameter of processing, microhardness and wear tests specimens were of (5×10) *mm* dimensions cut from the center of the stirring zone, and specimens for the tensile test were cut parallel to the longitudinal direction of FSP using the CNC milling machine mentioned above as shown in Fig.4. The dimensions and geometry of the tensile sample are shown in Fig.5 according to on the specifications given in ASTM standard E8M-011 of sub-size samples [15].

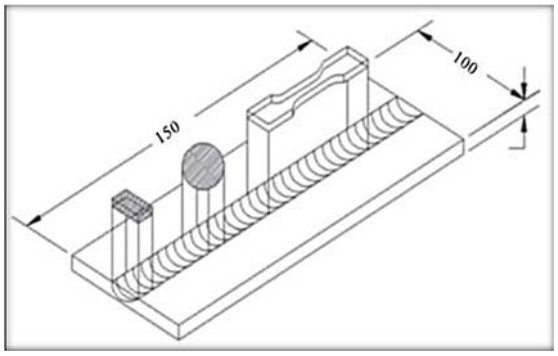

Fig.4. Specimen preparation for different tests in friction stir processed zone.

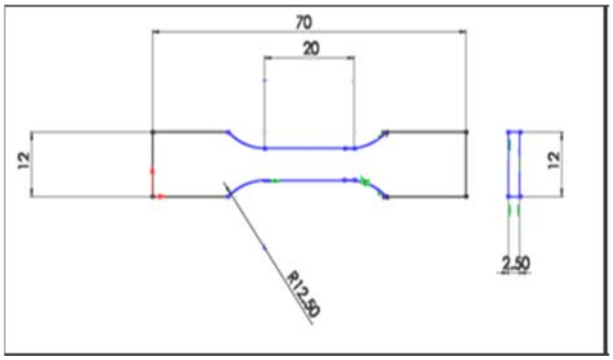

Fig.5. Tensile test sample.

4. Microhardness test and microstructure inspection

The specimens were examined using an optical microscope. Wet grinding was performed with water, and SiC sandpaper in variant grits of (*600*, *800*, and *1000*). Specimens were polished was done with *0.5m* diamond paste and a specific polishing cloth and lubricant. The etching process was performed on the specimens using Keller's reagent etching solution (composed of *95 ml* H2O, *2.5 ml* HNO3, *1.5 ml* HCL, and *1.0 ml* HF). Then the were specimens cleaned and dried. The information on the microstructure of processing specimens was obtained using an optical microscope. The Vickers hardness test was performed using a digital microhardness tester (Laryee, Mode HVS-1000). For *15 seconds*, a *200-gram* load was applied to the cross-section of the stirring zone in the friction stir processing direction.

5. Result and Discussion

5.1. Signal to Noise (SN) Ratio

The influence of FSP parameters on the tensile strength was estimated using S/N ratios and mean values for each factor of FSP (speed of rotation, traverse speed, hole depth, and mixing ratio of (B4C/SiO2) nanoparticles). A acceptable SN ratio was chosen to maximize the response; the S/N ratio for this study was carefully. The SN ratio is used to define the difference between the quality characteristics and the desired value using the Taguchi method. The effect of FSP parameters on tensile strength data has been investigated in this work. Table 5 shows the three levels of process parameters as per L9 orthogonal array, mean tensile strength, and matching S/N ratio.

Table 5. Signal to noise (S/N) ratios response table.

Experiment number	Tensile strength MPa	SN ratio	Mean values
1	*170*	*47.1967*	*229*
2	*166*	*47.0822*	*226*
3	*159*	*47.0050*	*224*
4	*167*	*47.0437*	*225*
5	*146*	*46.7691*	*218*
6	*173*	*47.2346*	*230*
7	*168*	*47.4214*	*235*
8	*178*	*47.1205*	*227*
9	*223*	*47.7121*	*243*

Evaluating the mean of each experiment will lead to a higher level of parameter combination, ensuring strong tensile strength in terms of experimental data. Figures 6 and 7 show charts that can be used to determine the highest process parameter level compliance to the largest S/N ratio and tensile strength.

With *1200 rpm*, *30 mm/min* travel speed, *2.5 mm* hole depth, and *1/2* of (B4C/SiO2) nanoparticles mixing ratio, the tensile strength is the highest. This result is due to the new microstructure with very fine grains resulting from the FSP, where the high rotational speed (*1200*) *rpm* reduces the particle size because it leads to large plastic deformation and homogenous distribution of nanoparticles. While the high linear speed limits the temperature increase, which leads to preventing the grain growth and their recrystallization, whereas the high depth of the holes allows the addition of a larger quantity of high-hardness ceramic nanoparticles.

5.2. Analysis of variance (ANOVA) for tensile strength

The analysis of variance was used to determine the FSP parameter's significance that affects the tensile strength of materials processed with friction stir processing. The F-test, named after Fisher, can be used to evaluate which of the parameters has a substantial impact on the tensile strength.

Table 6. ANOVA table for (S/N) ratios for tensile strength.

Source	DF	Seq SS	Adj SS	Adj MS	F	P %
Rotational speed	*2*	*0.226895*	*0.226895*	*0.113447*	*62.6*	*39.9*
Travers speed	*2*	*0.168898*	*0.168898*	*0.084449*	*46.58*	*30.2*
Holes depth	*2*	*0.069074*	*0.069074*	*0.03453*	*19.04*	*12.3*
Mixing ratio	*2*	*0.065138*	*0.065138*	*0.032569*	*17.96*	*11.3*
Residual error	*2*	*0.036261*	*0.036261*	*0.001813*		*6.3*
Total	*8*	*0.575685*				*100%*

Table 7. Rank of FSP parameters.

Level	Rotational speed	Travers speed	Holes depth	Mixing ratio
1	*47.09*	*47.22*	*47.18*	*47.23*
2	*47.02*	*46.99*	*47.28*	*47.25*
3	*47.42*	*47.32*	*47.07*	*47.06*
Delta	*0.40*	*0.33*	*0.21*	*0.19*
Rank	*1*	*2*	*3*	*4*

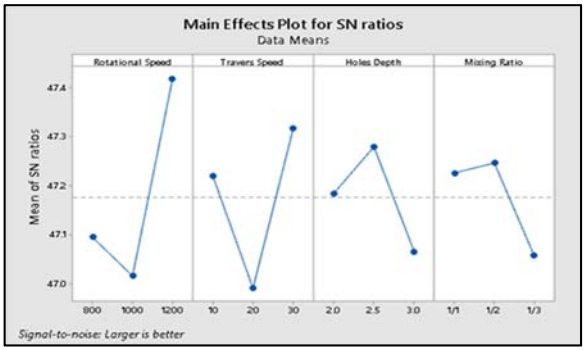

Fig.6. Plot of the main effect for SN ratios.

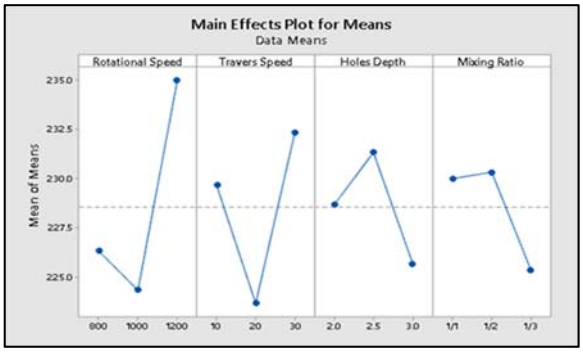

Fig.7. Plot of the main effect for mean tensile strength.

In general, when F is deemed high, the variation in process parameters has a significant effect on the quality features associated with the tensile strength. The ANOVA test findings show that the process parameters, rotation speeds, and traverse speed have a significant impact on the tensile strength with FSP. Table 6 shows that the analysis of variance (ANOVA) of tensile results shows that the speed of rotation is the most effective factor, accounting for *39.9* % of the total, followed by the traverse speed of *30.2* %, holes depth of *12.3* %, and mixing ratio *11.3* %.

5.3. Tensile test results

The tensile analysis showed that the base alloy tensile strength was higher than that of all samples submitted to FSP, as illustrated in Fig.8. The results of the tests show that an increase in linear and rotation speed leads to an increase in the tensile strength. The tensile strength was at its peak with a tool rotation speed of *1200 rpm* compared to unprocessed samples. It has been observed that increased tool rotation speed reduces tensile strength. These results are consistent with the reference [13].

A high rotational speed increases the stirring process in the stir zone (SZ) which leads to grain refinement, that explains why the minimum speed of rotation causes a drop in FSP tensile strength, whereas the maximum rotational speed generates a gain in tensile strength, resulting in a shorter exposure period to frictional heating. whereas a high traverse speed limits heat generation to allow grain recrystallization and limits grain growth. The hole depth and mixing ratio have a simple effect on the tensile strength as shown in Tab.6, but a high hole depth allows for more nanoparticles to incorporate in the metal matrix which may lead to agglomeration of these nanoparticles and a stress formation of concentration point.

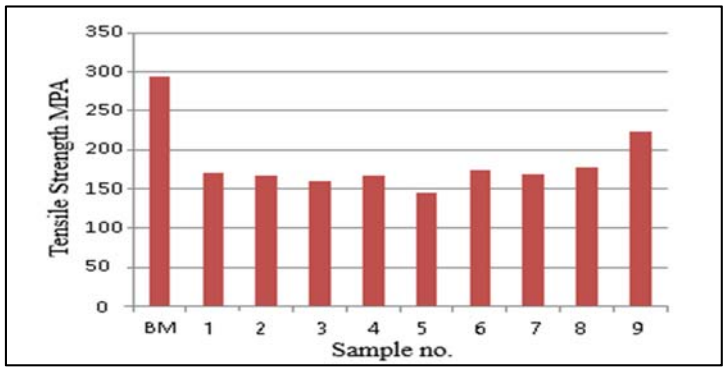

Fig.8. Base metal AA6061-T6 and samples of friction stir processing tensile strength.

5.4. Results of microhardness test

The distribution of Vickers-microhardness on a cross-section perpendicular to the direction of traverse for the sample submitted to FSP, generated at *1200 rpm* rotational speed, *30 mm/min* travel speed, *2 mm* hole depth, and at *1/3* B4C/SiO2 mixing ratio is shown. The hardness of the stir zone SZ was higher than that of the thermomechanically affected zone (TMAZ), heat affected zone (HAZ), and the base metal (BM) as shown in Fig.8. In the center of the stir zone, the maximum hardness was *155HV*. This is attributed to the precipitates of 2nd phase particles of Al3Mg2 phase in -Aluminum, and the existence of nanoparticles of extremely small size and high hardness compared to the base alloy. The nanoparticles enter the interspaces and it leads to an increase in density and a decrease in porosity, which in turn leads to an increase in hardness. and as well as the refining grain and dynamic, recrystallize in the stir zone.

In their tests of FSW welding aluminum alloys, several researchers [16, 17] confirmed similar findings. An analysis of variance (ANOVA) table shows that the rotational speed has a significant effect on the FSPed alloy hardness with a contribution ratio of *39.37*%, which may be due to the ultra-fine grain size generated during high rotational speed, while the second affected parameter was the mixing ratio of B4C/SiO2

nanoparticles with a contribution ratio of (*24.44*%) that may be due to the high hardness of ceramics nanoparticles and the good distribution of these nanoparticles through the Al matrix. Traverse speed, and holes depth has a contribution of (*18.94* and *14.45*) as shown in Tab.8, whereas Tab. 9 shows the rank of FSP parameters for the SN ratio. Figures 10 and 11 show the main effect plot for the S/N ratio and mean of microhardness.

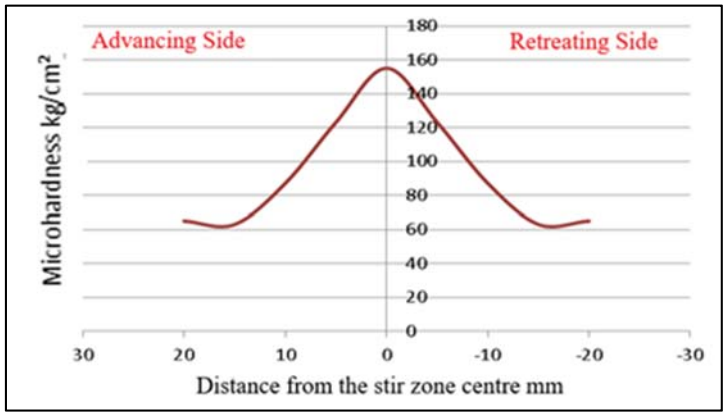

Fig.9. The distribution of microhardness across tool traverse direction at *1200 rpm* rotational, *30 mm* traverse speed, *2 mm* hole depth, and *1/3* mixing ratio.

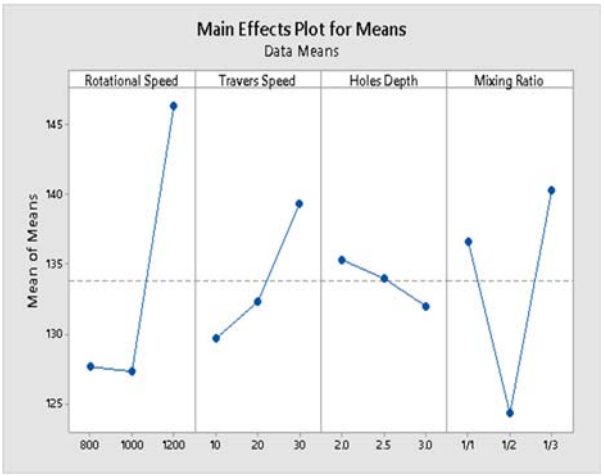

Fig.10. Main effect plot S/N ratios.

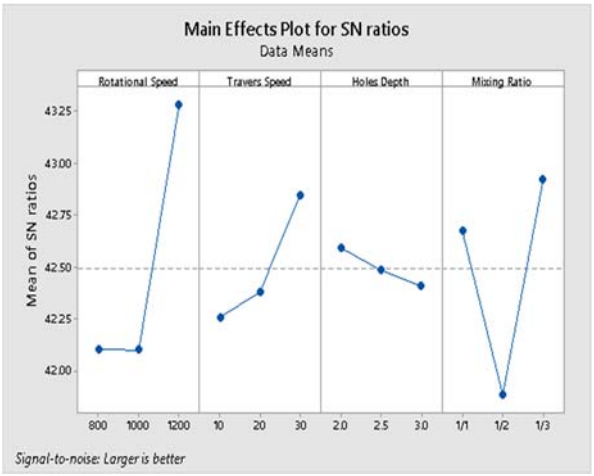

Fig.11. Main effect plot for mean hardness.

Table 8. ANOVA table for S/N ratios.

Source	DF	Seq SS	Adj SS	Adj MS	F	Contribution %
Rotational speed	*2*	*2.04978*	*2.04978*	*1.02489*	*28.2*	*39.37*
Travers speed	*2*	*0.98498*	*0.98498*	*0.49249*	*13.55*	*18.94*
Holes depth	*2*	*0.75226*	*0.75226*	*0.37613*	*10.35*	*14.45*
Mixing ratio	*2*	*1.27418*	*1.27418*	*0.63709*	*17.53*	*24.44*
Residual error	*2*	*0.14539*	*0.07269*	*0.03634*		*2.8*
Total	*8*	*5.20659*				*100 %*

Table 9. Rank of FSP parameters.

Level	**Rotational speed**	**Travers speed**	**Holes depth**	**Mixing ratio**
1	*42.10*	*42.26*	*42.59*	*42.68*
2	*42.10*	*42.38*	*42.48*	*41.88*
3	*43.28*	*42.85*	*42.41*	*42.92*
Delta	*1.18*	*0.59*	*0.19*	*1.04*
Rank	*1*	*3*	*4*	*2*

Table 10. Signal to Noise (S/N) ratio response table.

Experiment number	**Microhardness** *Kg/cm²*	SNR	MEAN
1	*128*	*42.1442*	*128*
2	*117*	*41.3637*	*117*
3	*138*	*42.7976*	*138*
4	*130*	*42.2789*	*130*
5	*127*	*42.0761*	*127*
6	*125*	*41.9382*	*125*
7	*131*	*42.3454*	*131*
8	*153*	*43.6938*	*153*
9	*155*	*43.8066*	*155*

Table 11. Experiments ranking for tensile strength and microhardness.

No. of test	Rotational speed *rpm*	Travers speed *mm/min*	Holes depth *mm*	Mixing ratio	Tensile strength MPa	Rank	Hardness *Kg/cm²*	Rank
1	*800*	*10*	*2*	*1/1*	*170*	*4*	*128*	*6*
2	*800*	*20*	*2.5*	*1/2*	*166*	*7*	*117*	*9*
3	*800*	*30*	*3*	*1/3*	*159*	*8*	*138*	*3*
4	*1000*	*10*	*2.5*	*1/3*	*167*	*6*	*130*	*5*
5	*1000*	*20*	*3*	*1/1*	*146*	*9*	*127*	*7*
6	*1000*	*30*	*2*	*1/2*	*173*	*3*	*125*	*8*
7	*1200*	*10*	*3*	*1/2*	*168*	*5*	*131*	*4*
8	*1200*	*20*	*2*	*1/3*	*178*	*2*	*153*	*2*
9	*1200*	*30*	*2.5*	*1/1*	*223*	*1*	*155*	*1*

5.5 Results of wear test

The weight loss method was utilized to define the wear rate using pin on disk technique. Specimens were weighed before and after the test, and the wear rate was obtained according to the following equation [18].

$$Ws = \frac{\Delta m}{L \cdot P \cdot F}$$

where Ws is wear rate (gm/cm), Δm – loss of weight, L – sliding distance (cm), P – material density (g/cm), F – applied load (N).

The wear test was carried out under dry sliding conditions by changing the applied load (*5*, *10*, *15*, and *20*) *N*, at fixed sliding time (*20*) *min*, sliding speed (*510*) rpm, and distance of (*5*) cm, whereas the hardness of steel disc was *32 HRC* as shown in Fig.12.

The rate of wear tends to increase as the load increases at a constant time and speed of sliding. Figure 13 shows that the wear behavior is the same for all specimens, and it also depicts 3 wear regions: mild, transition, and severe wear. The wear behavior changes from mild to severe wear type over *10 N* load. The rate of wear of the FSP samples was lower than that of the unprocessed Al alloy AA6061-T6 due to the presence of ceramics nanoparticles, and fine grains structures resulting from the severe plastic deformation and dynamical recrystallization that occurred during the FSP.

Fig.12. Pin on disk device.

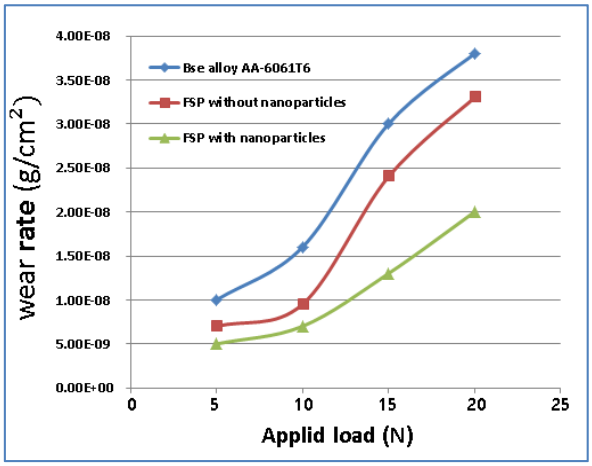

Fig.13. The effects of applying loads on the wear rate.

5.6. Microstructure results

The microstructure characterization of FSP samples at optimum factors (*1200 rpm*, *30mm/min*, *3 mm*, and *1/1*) is illustrated in Fig.14 (a, b, c, and d).

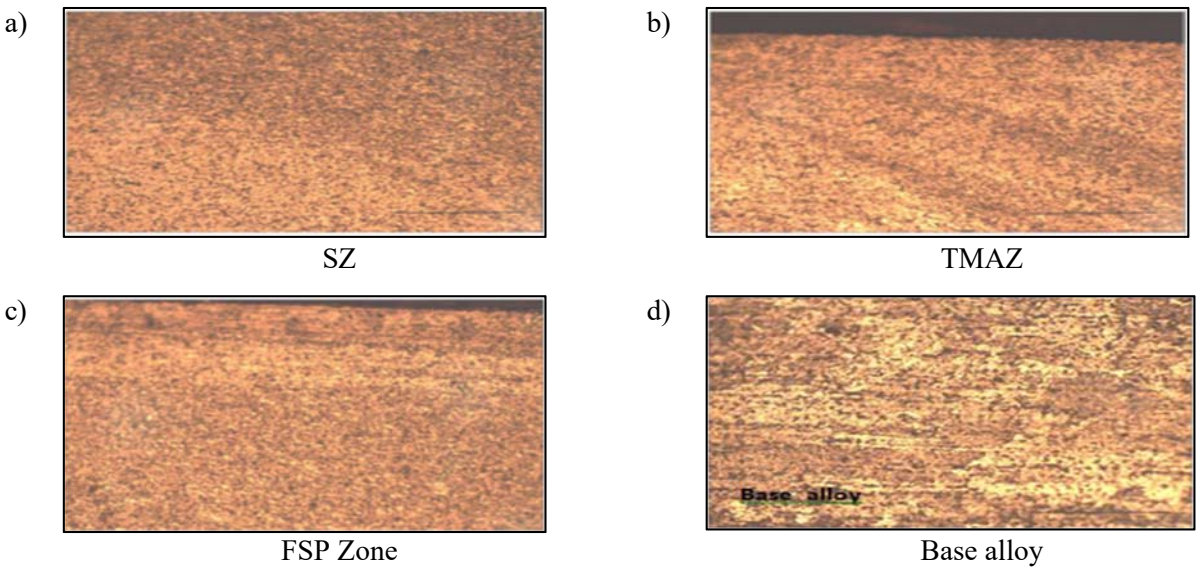

Fig.14. FSP sample microstructure at optimum parameters at 100x; a) stir zone (SZ) and thermomechanically affected zone (TMAZ), b) Union rings in (TMAZ), c) friction stir processing zone (FSPZ), d) AA6061-T6 Al alloy.

The FSP sample has 4 main zones: stirring zone (SZ), which is the zone that is processed thermo-mechanically with very fine grain size and homogenized structure or equiaxed grains (Fig.14a), thermo-mechanically affected zone (TMAZ), which is a region where the grain was lengthened as a result of thermo-mechanical deformation in the shape of onion rings as shown (Fig.14b), FSP zone (Fig.14c), the heat affected-zone (HAZ), which has the same grain structure as the base metal (BM) or Al alloy 6061-T6 (unaffected metal), is the zone that is not altered by the friction stir process, such microstructures have ultra-thin Al3Mg2 phase 2nd phase particles that are uniformly dispersed in -Al (Fig. 14d).

Other physical tests such as FE-SEM, and XRD wear were conducted to study the microstructure and to make sure that the nanoparticles were uniformly distributed in the Al matrix surface composite. The SEM test shows that hybrid nanoparticles of SiO2 and B4Cwere distributed uniformly as shown in Fig.15, while the XRD test shows the existence of AL3MG2 phase and the residual stress as shown in Fig.16.

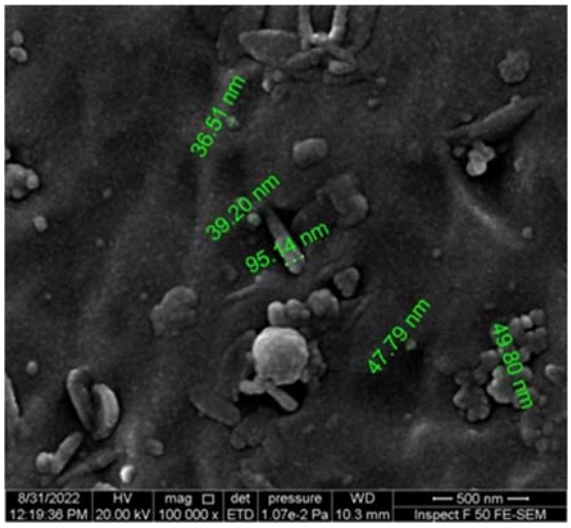

Fig.15. FE-SEM micrographs of AA6061-T6 sample reinforced by nanoparticles.

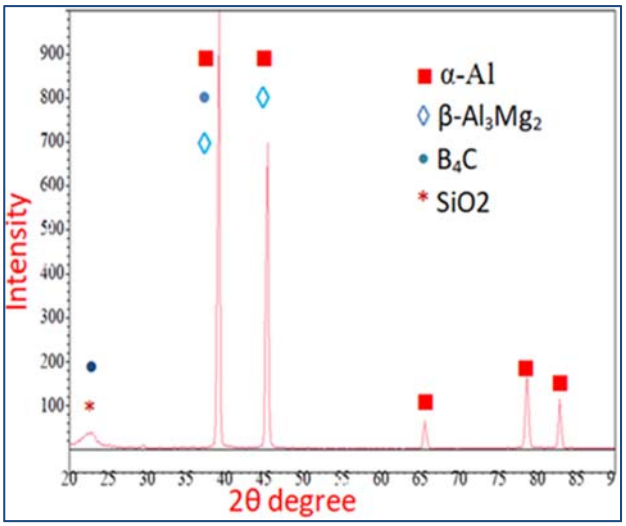

Fig.16. XRD analysis of FSP reinforced with nanoparticles.

6. Conclusions

Results showed that the hybrid addition of SiO2 and B4C nanoparticles to AA6061-T6 aluminum alloy enhanced mechanical properties such as microhardness and wear resistance that was due to the very fine grain size obtained after friction stir processing and the homogenized distribution of nanoparticles on the surface of the alloy. Other observations were:

- The ideal FSP parameters for tensile strength were found to be a rotational speed of *1200 rpm*, traverse speed of *30 mm/min*, hole depth of *2.5 mm*, and *1/2* mixing ratio of SiO2/B4C hybrid nanoparticles, while for microhardness they were as follows rotational speed of *1200 rpm*, traverse speed of *30 mm/min*, hole depth of 2 mm, and *1/3* mixing ratio of SiO2/ B4C hybrid nanoparticles
- As the rotational and traverse speed increased, the tensile strength increased due to the refining grain and the existence of precipitates (Al3Mg2) dispersed in the Al matrix,
- The stir FSP zone had microhardness higher than HAZ and TMAZ.
- From the ANOVA table of tensile strength, it was discovered that the speed of rotation has the highest contribution percentage (*39.9* %), and the travel speed (*30.2* %).
- The ANOVA table of microhardness, reveals that the rotation speed has the highest contribution percentage (*39.37* %), and the travel speed (*24.44* %).
- The wear behavior changes from mild to severe wear type over *10 N* load.

- The rate of wear of the FSP samples was lower than that of the unprocessed AA6061-T6 due to the presence of ceramics nanoparticles.

Acknowledgment

This work was supported by the State Company for Automotive and Equipment Industry (SCAEI) supervised by the Government of the Republic of Iraq.

Nomenclature

DOE – design of experiment
TMAZ – thermomechanical affected zone
HAZ – heat affected zone
SZ – stir zone
ANOVA – analysis of variance
TMT – thermomechanical treatment
HPT – high-pressure torsion
ECAP – equal channel angular procedure
ARB – accumulative roll bonding
FSP – friction stir processing
CNC – computer numerical control
ASTM – American Society for Testing and Material
SN – signal to noise ratio
DF – degree of freedom
SS – summation square
MS – mean square
BM – based matel
FSW – friction stir welding
SEM – scanning electron microscopy
XRD – X-ray diffraction

References

1. Saravanan C., Subramanian K., Krishnan V.A. and Narayanan R.S. (2015): *Effect of particulate reinforced aluminum metal matrix composite-a review.*– Mechanics and Mechanical Engineering, vol.19, No.1, pp.23-30.
2. Kishan V., Devaraju A. and Lakshmi K.P. (2017): *Influence of volume percentage of NanoTiB2 particles on tribological & mechanical behavior of 6061-T6 Al alloy nano-surface composite layer prepared via friction stir process*.– Defence Technology, vol.13, No.1. pp.16-21.
3. Venkateswarlu G., Davidson M.J. and Sammaiah P. (2014): *Effect of friction stir processing process parameters on the mechanical properties of AZ31B Mg alloy*.– Manufacturing and Industrial Engineering, vol.13, No.1-2, pp.1-5.
4. Daniolos N.M., Pantelis D.I. and Sarafoglou P.I. (2011): *AA7075 /Al2O3 surface composite materials fabrication using friction stir processing*.– in: 2nd International Conference of Engineering Against Fracture (ICEAF II), Mykonos, GREECE.
5. Deepak D., Sidhu R.S. and Gupta V. (2013): *Preparation of 5083 Al-SiC surface composite by friction stir processing and its mechanical characterization*.– International Journal of Mechanical Engineering, vol.3, No.1, pp.1-11.
6. Liu Q., Ke L., Liu F., Huang C. and Xing L. (2013): *Microstructure and mechanical property of multi-walled carbon nanotubes reinforced aluminum matrix composites fabricated by friction stir processing*.– Materials & Design, vol.45, No.1, pp.343-348.

7. Ma Z. (2008): *Friction stir processing technology: a review*.– Metallurgical and materials Transactions A, vol.39, No.3, pp.642-658.
8. Karna S.K., Singh D.R.V. and Sahai D.R. (2012): *Application of Taguchi method in indian industry*.– International Journal of Emerging Technology and Advanced Engineering, vol.2, No.11, pp.387-391.
9. Kwon Y., Shigematsu I. and Saito N. (2003): *Mechanical properties of fine-grained aluminum alloy produced by friction stir process*.– Scripta Materialia, vol.49, No.8, pp.785-789.
10. Elangovan K. and Balasubramanian V. (2007): *Influences of pin profile and rotational speed of the tool on the formation of friction stir processing zone in AA2219 aluminum alloy*.– Materials Science and Engineering: A, vol.459, No.1-2, pp.7-18.
11. Shafiei Zarghani A., Kashani Bozorg S. and Zarei-Hanzaki A. (2008): *Ultrafine grained 6082 aluminum alloy fabricated by friction stir processing*.– International Journal of Modern Physics B, vol.22, No.18n19, pp.2874-2878.
12. El-Rayes M.M. and El-Danaf E.A. (2012): *The influence of multi-pass friction stir processing on the microstructural and mechanical properties of Aluminum alloy 6082*.– Journal of Materials Processing Technology, vol.212, No.5, pp.1157-1168.
13. Muna K. Abbassa and Noor Alhuda B. Sharhana, (2019): *Optimization of friction stir processing parameters for Aluminum alloy (AA6061-T6) using Taguchi method*.– Al-Qadisiyah Journal for Engineering Sciences, vol.12, pp.001-006.
14. Noor Zaman Khan, Zahid A. Khan, and Arshad Noor Siddiquee (2015): *Effect of shoulder diameter to pin diameter (D/d) ratio on tensile strength of friction stir welded 6063 aluminium alloy*.– Materials Today: Proceedings., vol.2, Iss.4-5, pp.1450-1457.
15. Yuvaraj N. and Aravindan S. (2015): *Fabrication of Al5083/B4C surface composite by friction stir processing and its tribological characterization*.– Journal of materials research and technology, vol.4, No.4, pp.398-410.
16. Abbass M.K. and Abd H.H. (2013): *A comparison study of mechanical properties between friction stirwelding and TIG welded joints of aluminum alloy (Al 6061-T6)*.– Engineering and Technology Journal, vol.31, No.14, pp.2701-2715.
17. Abbass M.K. and Raheef K.M. (2018): *Effect of welding parameters on mechanical properties of friction stir lap welded joints for similar aluminum alloys (AA1100-H112 & AA6061-T6)*.– Journal of Engineering and Sustainable Development, vol.22, No.2, pp.60-71.
18. Kang Yang, Xiaoliang Shi, Wenzheng Zhai and Ahmed M. Ibrahim (2015): *Wear rate of TiAl matrix composite containing 10wt. %Ag predicted by Newton interpolation method*.– RSC Advances, vol.5, Iss.82, pp.67102-67114.

Received: June 23, 2022
Revised: October 15, 2022